The Holocene 13,3 (2003) pp. 433–446

Lateglacial and Holocene environmental changes in Portuguese coastal lagoons 1: the sedimentological and geochemical records of the Santo André coastal area

Maria da Conceição Freitas,[1]* César Andrade,[1] Fernando Rocha,[2] Colombo Tassinari,[3] José Manuel Munhá,[1] Anabela Cruces,[1] Jesus Vidinha[2] and Carlos Marques da Silva[1]

([1]Centro de Geologia da Universidade de Lisboa, Bloco C2, 5° Piso, Campo Grande, 1749-016 Lisboa, Portugal; [2]Departamento de Geociências, Universidade de Aveiro, 3810-193 Aveiro, Portugal; [3]Universidade de S. Paulo, Instituto de Geociências – Centro de Pesquisas Geocronológicas, S. Paulo, Brasil)

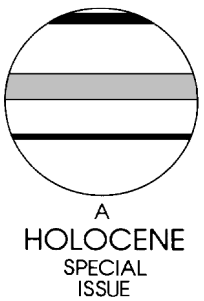

Abstract: The sedimentological and geochemical study of a core corresponding to sedimentation in the Santo André lowland since 14 000 BP allowed the reconstruction of environmental changes of this area and discussion of the relative importance of local versus global forcing factors responsible for its evolution. The pre-Holocene section of the core represents terrestrial sedimentation in a fluviatile environment, contemporaneous of a low sea level and a distal shoreline. Sediment inputs were terrestrial and resulting from intensive weathering and high erosion rate in the adjacent watershed. During the Early Holocene (*c.* 10 020 to 5380 BP) the sea invaded this lowland and defined an open marine shallow environment corresponding to a wide gulf which has been disturbed by multiple terrestrial inputs that might have been induced by massive episodes of fluvial discharge. The first symptoms of confinement were noticed close to 5400 BP, and *c.* 5380 BP a major environmental threshold occurred (possibly reflecting the marked deceleration of the sea-level rise rate) corresponding to the establishment of an efficient detrital barrier that completely isolated the bay and changed this lowland into a closed coastal lagoon. After 5380 BP, the lagoonal environment evolved as a function of local forcing factors, among which the frequency and efficiency of exchanges with the ocean predominate: until *c.* 3570 BP the lagoon was restricted, fed by fresh water and terrestrial sediment inputs; a second episode of lagoonal sedimentation lasts until *c.* 1620 BP, reflecting brackish conditions and increase in marine influence due to a reduced efficiency of the barrier. The upper section of the core represents the final stages of filling of the lagoonal margin by fluvial activity. Human settling and intervention in the barrier are possible causes of a short-lived return to brackish conditions recorded in the uppermost sediment unit of the core and of the dramatic increase of the sedimentation rates.

Key words: Palaeoenvironmental reconstruction, coastal evolution, Portugal, lagoon, textural proxies, mineralogical proxies, chemical proxies, strontium isotopes, Lateglacial, Holocene.

Introduction

It is widely accepted that most of the present-day European coastal lagoons have formed after 7000 BP where estuaries or coastal embayments flooded by the Holocene transgression have become enclosed by detrital barriers, which differentiated as a sequel of the fast decelerating rate of sea-level rise resulting from the melting of the last Pleistocene continental ice. Closing of the shore appears to have been a widespread response to increased stability in littorals free from significant postglacial isostatic rebound. This is confirmed by the mid- and late-Holocene geological record of Portuguese coastal lagoons which has been studied during the last decade for palaeoenvironmental reconstruction of that time period; these studies rely on multidisciplinary approaches and the interpretations are based on present-day analogues and comparative modelling of the microscale behaviour of these systems

*Author for correspondence (e-mail: cfreitas@fc. ul.pt)

10.1191/0959683603hl636rp

(Freitas *et al.*, 1993; Freitas and Andrade, 1994; Freitas, 1995; Bao *et al.*, 1999). In contrast, the palaeoenvironmental changes of those lowlands during the Lateglacial and early Holocene are rare and limited in scope (cf. Mateus, 1992; Queiroz and Mateus, 1994).

Sea-level data with interest for the Portuguese coast are sparse (Clark *et al.*, 1978; Dias, 1985; 1987) and generally lack adequate resolution or include a high-stand above the present level (*c.* 2000 BP) that has never been demonstrated (Bao *et al.*, 1999). However, the critical change of sea-level rise rate *c.* 5000 BP is a common feature in this literature.

This paper corresponds to a pilot project and presents a contribution to the first detailed and multidisciplinary study of a continuous core taken from the lowland of Santo André (southwestern coast of Portugal) that extends from 14 000 BP until present. Future work in this lowland might refine the interpretation presented in this paper. Yet the internal consistency found between distinct environmentally sensitive proxies and coherence with other reconstructions established in similar environments along the same coast suggest that the main evolutionary stages here defined stand on their own merit despite being supported by the study of one single core. Due to its geomorphological setting, this area contains a geological record that provides key elements to the understanding of the post Lateglacial evolution of the Southwestern Iberian coast. This study aims to reconstruct the environmental changes experienced at a local scale and to sort out the relative importance of local versus global forcing factors as major controls of its evolution using sedimentological and geochemical proxies. The palaeoecological approach to this core is explained in the papers by Cearreta *et al.* (this issue) and Santos and Goñi (this issue).

The study area

The Santo André coastal area is located some 80 km south of Lisbon, in the southern half of the Tróia-Sines coastal bay (Figure 1A), a high mesotidal coast according to Hayes (1978). This section of the coast is dominated by long-period west-northwestern swell and is occasionally disturbed by short-lived but violent western or southwestern storms. The coast is pronouncedly arcuate, similar to the equilibrium shape described by Silvester (1974). This explains why the yearly net littoral drift volume is small in spite of a high wave-energy regime.

The main geomorphologic feature of this area is the Santo André coastal lagoon, a closed lagoon according to Nichols and Allen (1981). The lagoon is separated from the ocean by a continuous reflective sand barrier consisting of multiple sand ridges (defining a ridge-and-swale morphology) in its southern section (Figure 1B). These ridges trend obliquely and merge with the present-day beach-foredune system, progressively decreasing the width and complexity of the barrier towards the north where it reduces to a single detached beach. In this location, the barrier may occasionally breach during storms and a channel has been artificially and regularly cut since at least the seventeenth century, to promote water exchange, prevent eutrophication and drain the tributary alluvial plains, reclaimed for grazing (cf. Cardoso, 1747; Silva, 1869). This is usually carried out during spring tides in Easter and with annual periodicity. The inlet is ephemeral and evolves naturally until complete silting up in a matter of weeks, essentially trough wave-driven cross-shore sediment transfer.

The flooded surface of the Santo André lagoon changes between 1.7 and 2.5 km^2, as a function of rainfall and drainage induced by barrier breaching. The average depth and stored volume of water vary seasonally, the maximum depths (observed in tidal channels close to the barrier) not exceeding 4 m. The salinity ranges seasonally between 35‰ during open-inlet periods and brackish when the lagoon is isolated from the ocean.

This lagoon displays a complex plan shape and consists of a central main basin and a number of confined N–S elongated troughs (locally designated by 'Poços' and associated with the ridge-and-swales) that are connected to the major water body by restricted channels (Figure 1B). The lagoon collects fluvial inputs of water and sediment of two main drainage networks that outlet from the east and south, through wide alluvial plains extensively choked with sediment.

Methods

A continuous 25.45 m long sediment core was taken in June 1998 from the alluvial plain of Badoca in a distal location relative to the tidal inlet (Figure 1B). The coring site was coordinated and connected to the UTM grid and Portuguese vertical Datum (mean sea level – m.s.l.). In this paper positive and negative elevation figures refer to heights and depths above and below m.s.l. respectively. The borehole (LSA – UTM 29SNC18601511, elevation +2.743 m) has been performed using 50 to 75 mm diameters and 1 m long Shelby samplers, driven by hydraulic pressure and operated inside a cased borehole. The core reached the basement (locally represented by Miocene sediments) at –21.33 m. The coring site has been chosen after a preliminary regional lithostratigraphic survey consisting of the retrieving and study of a set of 23 short cores (maximum length *c.* 9 m), which were described in the field and sampled for dating purposes.

In the laboratory, the core was opened longitudinally and described macroscopically. Both halves were then subsampled for dating, sedimentological, geochemical and palaeoecological studies. Samples were oven-dried at 60°C and split for further processing. Organic matter (O.M.) content was determined using about 1 g of dried sediment through oxidation with potassium-dichromate followed by titration using iron-sulphate (Standard E-201, LNEC, 1967). Grain-size analysis was undertaken by standard sieving on sediment coarser than 63 μm and the undersized fraction has been studied using a Fritsch laser particle analyser. Sediment classification follows Larsonneur (1977); the dimensional and sorting textural classification of sand follows Friedman and Sanders (1978). The carbonate content (bioclasts) was determined by weight difference before and after digestion with diluted hydrochloric acid.

The mineralogical composition of both the fine-grained fraction (<63 μm) and clayey fraction (<2 μm) was determined in a set of 66 samples using x-ray diffraction, according to the methodology of Rocha (1993). The correspondent diffractograms allowed a semi-quantitative interpretation, following criteria recommended by Schultz (1964) and Thorez (1976).

Thirty-five whole rock (dried) sediment samples were analysed by fusion inductively coupled plasma emission/mass spectrometry (ICP/MS) and instrumental neutron activation analysis (Activation Laboratories Ltd., Canada) for major and several trace elements (Table 1). Out of these, 19 samples were further analysed for strontium isotopes at the Geochronological Research Center of the University of São Paulo (Brasil). Strontium isotopic analysis were carried out on a multicollector Finnigan-Mat 262 mass spectrometer using standard methods according to the analytical procedures described by Kawachita (1972); isotopic ratios were normalized to $^{86}Sr:^{88}Sr = 0.1194$, giving a mean $^{87}Sr:^{86}Sr$ for NBS987 standard of 0.71028 ± 0.00006 (2σ).

Sediment samples collected for dating consisted of thin (1–2 cm) slices of organic muds and more rarely wood. Samples were dated by standard accelerated mass spectrometry (AMS) ^{14}C radiometric determination at Beta Analytic Inc., USA. Calibration of radiocarbon dates was performed according to Vogel *et al.* (1993), Talma and Vogel (1993) and Stuiver *et al.* (1993).

Results

The sedimentological and geochemical study of core LSA together with the palaeoecological approach (cf. Cearreta *et al.*, this issue, and Santos and Goñi, this issue) allowed the definition of four major lithostratigraphical units (units I to IV) resting over Miocene basement.

Texture, calcium carbonate and organic matter content

Basement

The basement was sampled between –22.71 and –21.33 m and consists of a greenish, very compact, micaceous muddy to silty fine sand (according to Folk, 1974) with few scattered pebbles. No O.M. was detected and the carbonate content is very low (< 3%) (Figure 2). Throughout this section the kaolinite:illite ratio (K:I) is consistently low (Figure 5); the contents in phylosilicate (Phy), opal C/CT and K-feldspar are high, while quartz and plagioclase are low (Figure 4). These characteristics change abruptly when the sharp surface corresponding to its upper boundary gives way to the lower sediments of the Quaternary section of the core.

Unit I (–21.33 to –11.51 m)

This unit consists of a monotonous series of decimetric layers of sand and muddy sand alternating with mud and sandy mud (Figure 3A). The boundaries separating layers are usually gradual and diffuse. The sandy fraction is generally medium to coarse, moderately to poorly sorted and negatively skewed, suggesting the presence of small contributions of coarser lag. Throughout this unit the clay:silt ratio is variable, most samples falling in class III of Pejrup (1988), regardless of the sand content (Figure 3B). Mica flakes (muscovite) and fermented plant remains (more rarely charcoal) were recognized in small amounts throughout this unit. Bioclasts are present as whole shells and shell debris of bivalves and gastropods (Figure 2).

Subunit IA (–21.33 to –18.06 m)

The coarsest layer of the whole core was found close to the base of this subunit and consists of poorly sorted, negatively skewed very coarse to pebbly sand (containing quartz pebbles) resting over a micaceous, reddish, medium sand horizon. Grit or fine pebble clasts of slate are frequently found dispersed (especially below –18.7 m) within both the sandy and muddy layers. The O.M. content is less than 1% and bioclasts less than 3% of the total sample (Figure 2). The latter are represented by shell debris of bivalves (essentially of the family Cardiidae) and whole shells of *Parvicardium* sp.

Subunit IB (–18.06 to –14.26 m)

Within this subunit the sand content and the mean diameter of the sand generally increase upcore. The major textural contrast with the underlying subunit is the absence of the lithic coarse components. Bioclasts contribute less than 10% to the total sample (averaging 6%) and are represented by shell debris and whole shells – *Rissoa* sp., *Corbula gibba*, *Cerastoderma* sp. and undetermined Cardiidae, Bivalvia and Gastropoda. The O.M. content is less than 2% of the total sample. Samples correspondent to this interval show the higher clay:silt ratio, clustering around 1:1 (Figure 3B).

Subunit IC (–14.26 to –11.51 m)

It consists of an essentially muddy deposit comparatively enriched in O.M., containing two thick layers of less organic coarser sediment. The basal contacts of the sand are sharp and the upper boundaries between the sand and the mud gradual. Bioclasts usually exceed 8%, averaging 12% of the total sample and show large diversity (*Caecum imperforatum*, *Chrysallida* sp., *Bela* sp., *Nassarius* sp., *N. mamillatus*, *Ocinebrina aciculata*, *Bittium reticulatum*, *B. latreillei*, *Pusillina* sp., *P. lineolata*, *Hyala vitrea*, ?*Jujubinus* sp., *Hydrobia* sp., *H. ulvae*, *Turbonilla* sp., *Rissoa* sp., *Cerastoderma* cf. *edule*, *Corbula gibba*, *Chlamys* sp., *Parvicardium exiguum*, *Abra alba*, *Dosinia* sp., *Tapes* cf. *decussates*, undetermined Cardiidae, Bivalvia and Gastropoda and gastropod opercula. The O.M. content is variable with peak values of about 4.5 to 7.5%, generally associated with low sand content (Figure 2).

Unit II (–11.51 to –2.48 m)

This unit consists essentially of brown to grey (frequently organic) muds faintly laminated and containing occasional laminae of sand more frequent in its upper section (Figure 2). Throughout this unit bioclasts are abundant (usually >20%; Figure 2) whole shells (bivalves and gastropods) predominating over shell debris.

Subunit IIA (–11.51 to –8.26 m)

This subunit displays a very uniform texture; it is composed almost exclusively of muds (94–99% silt + clay; Figure 3A) and

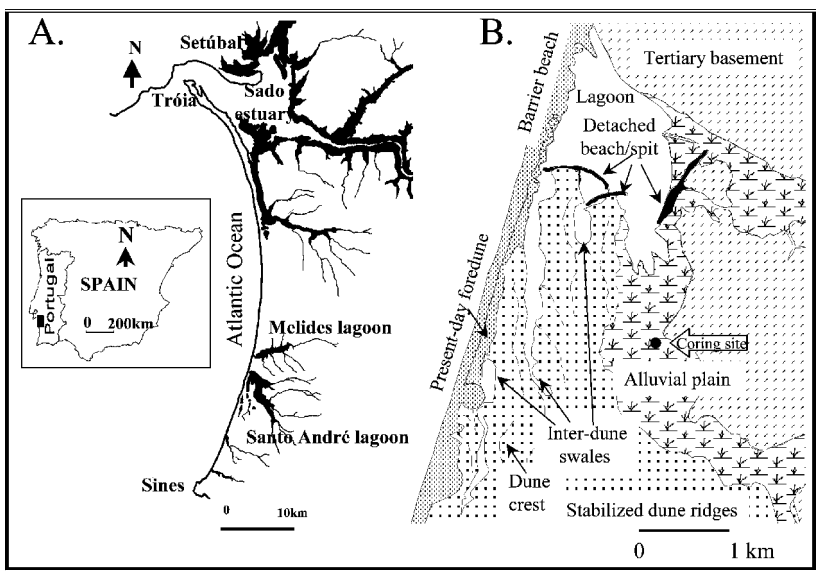

Figure 1 (A) Location of the study area in Portugal and in the Tróia-Sines coast. (B) Geomorphological sketch of the Santo André area and location of coring site LSA.

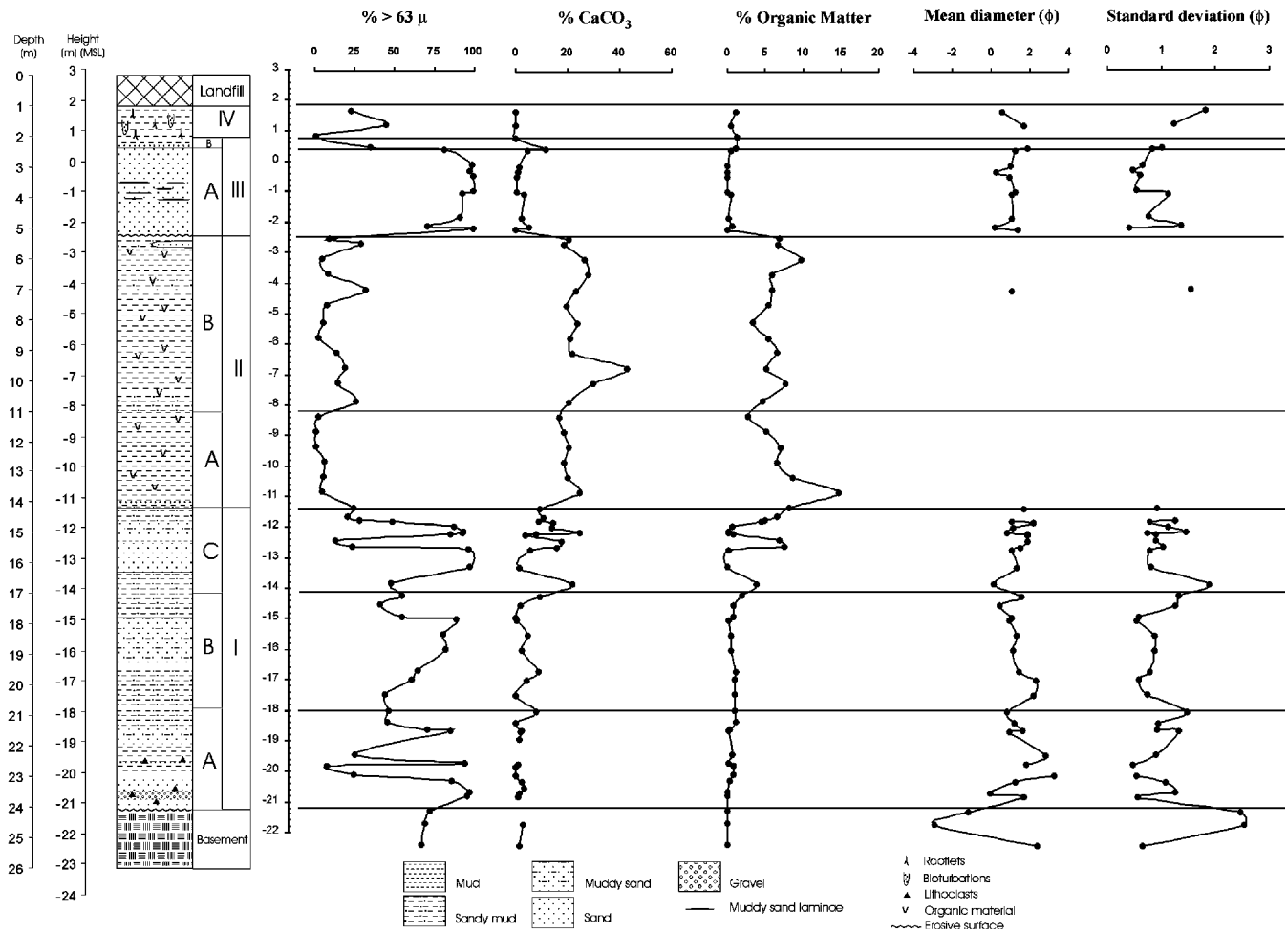

Figure 2 Sedimentological column and vertical profiles of textural and compositional attributes of sediments from the core LSA.

O.M. content ranges between 3 and 15%, generally decreasing upwards. Close to the contact with subunit IC a few sandy laminae (medium sand, moderately sorted) repeat textural attributes of the top of subunit IC (Figure 2). Bioclasts range between 17 and 25% of the total sample, yet diversity is low: ?*Scrobicularia* sp. *Cerastoderma* sp. and debris of undetermined Bivalvia and Gastropoda.

Subunit IIB (–8.26 to –2.48 m)

Although still dominated by mud, the >63 μm content is more variable than in the underlying subunit (2 to 28%) but it is always lower (about 1/3) than the coarse content of unit I. The sand (medium to coarse, poorly sorted) is generally dispersed within the mud or (occasionally) defines thin laminae. O.M. content varies ±2% around an average figure of 7%, significantly higher than in subunits IA and IB (Figure 2). Bioclasts range between 19 and 43%, the higher content found in the sequence: *Hydrobia* sp., *H.* cf. *stagnorum*, *Rissoa* sp., *Nassarius mamillatus*, *Bittium reticulatum*, *Planorbis* sp., *Physella* sp., *Scrobicularia plana*, *Cerastoderma* sp., *C. edule*, *Corbula gibba* and debris of undetermined Cardiidae, Bivalvia and Gastropoda.

Unit III (–2.48 to +0.74 m)

This unit is essentially made of laminated sand, generally exceeding 90% of the total sample, topped by 35 cm of sandy mud and muddy sand.

Subunit IIIA (–2.48 m to +0.39 m)

This subunit essentially consists of coarse to medium, moderately to moderately well sorted sand. Between –0.76 and –1.31 m several distinct centimetric laminae of organic sand were found, which are exemplified by sample collected at –1.05 m with an O.M. content of 0.5%, but showing no further textural contrast (Figure 2). Transition with subunit IIB is quite sharply marked in the core by an erosive surface. Bioclasts content is very low, less than 5%, and represented by rare whole *Cerastoderma* sp. and debris of undetermined Cardiidae, Bivalvia and Gastropoda.

Subunit IIIB (+0.39 to +0.74 m)

This subunit establishes gradual transition to upper unit IV: there is an increase in the muddy fraction (19 to 65%), in the bioclasts content (5 to 12%) and in the O.M. content of the total sample (0.5 to 1.2%) (Figure 2). Bioclasts are represented by rare whole *Cerastoderma* sp. and debris of undetermined Cardiidae and Bivalvia. The sandy fraction is arranged in a fining upward sequence.

Unit IV (+0.74 to +1.74 m)

This unit consists of inorganic (O.M. content about 1%) brown mud to sandy mud (Figure 3A) with numerous plant remains, and is topped by 1 m of landfill. The sediment lacks any internal structure, with the exception of frequent vertical sand-filled bioturbations associated with rootlets. Sand is medium to coarse, moderately to poorly sorted (Figure 2).

Clay mineralogy

The downcore evolution of the mineralogical parameters of the fine-grained and clay fractions of the cored sediments (Figures 4 and 5), in particular clay mineral assemblages, allowed the characterization of the distinctive units/subunits. Unit I presents the highest abundance of chlorite, K-feldspar, plagioclase and phyllosilicates, opal C/CT occurring in significant proportions at a few horizons. Maximum contents of phyllosilicates (in particular

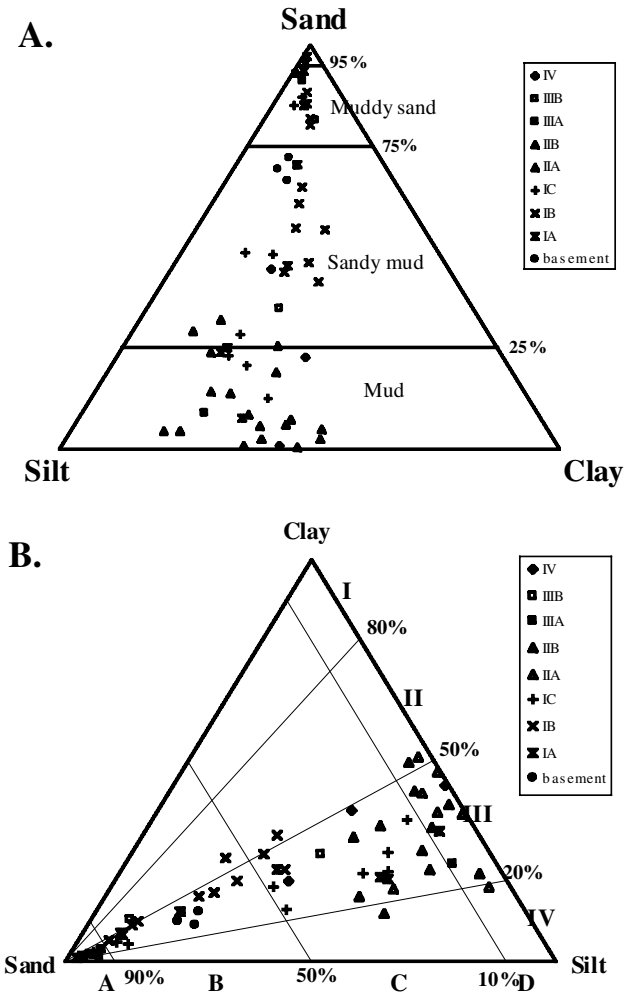

Figure 3 Plots of sediment samples in the diagrams of (A) Larsonneur and (B) Pejrup.

smectite) were observed in subunit IB, while chlorite concentrates preferably in subunit IA. Within subunits IA and IB the K:I ratio is consistently above the average figure obtained for the whole core. The proportion of chlorite and smectite drops in subunit IC, while illite clearly increases at the expense of the remnant mineralogical assemblage. Both pyrite and anhydrite progressively increase in abundance to the top of unit I. Transition to unit II is marked by the dropping of phyllosilicates and feldspars in what concerns the fine-grained fraction and of smectite and K:I ratio in what concerns the clay fraction; simultaneously an increase of pyrite is noticed, which exhibits the highest values of the whole core (particularly in subunit IIB). Transition between subunits IIA and IIB is marked by a dolomitic episode. The K:I ratio drops from bottom to top of subunit IIA and reverses this trend throughout IIB. The smectite:chlorite ratio increases from subunit IIA to IIB. Transition to unit III is marked by an increase of abundance of phyllosilicates (in particular smectite) and K-feldspar, while pyrite exhibits a reverse trend. The K:I ratio varies along this unit but no distinct trend is noticed. In unit IV, phyllosilicates (in particular chlorite), K-feldspar and pyrite reduce abundance and smectite keeps the high values of the previous subunit IIB, almost matching the proportion of kaolinite. The plagioclase content and the K:I ratio increase. The Kubler crystallinity index (Kubler, 1964) displays a quite uniform profile along the whole core with the exception of a positive peak in subunit IIA, meaning lower crystallinity.

Geochemistry

Major and trace element compositions of the analysed Santo André core samples are provided in Table 1. In general, observed downcore geochemical variations show distinct breaks which correspond with the boundaries of the different units or subunits. Downcore Si and Ca concentration changes reflect variations in relative proportions of sand and carbonate components; these variations are better emphasized by normalization relative to Al. Thus, Si:Al ratios reflect variations in sand content (Figure 6): unit II shows the lowest values and the highest homogeneity of this ratio, in clear contrast with the adjacent units. Ca:Al (Figure 6) essentially mirror the total carbonate content, and the maximum values of this ratio correspond to shell-rich laminae. All together, these three major elements (Si, Al, Ca) primarily reflect the lithological and to some extent textural heterogeneity found along the core. Sr:Al behaves like Ca:Al (Figure 6), whereas Th and rare earth elements (REE) abundance (Table 1) follow Al concentrations on displaying a strong positive correlation ($R^2_{Th} = 0.91$; $R^2_{La} = 0.89$) with silt + clay (<63 μm fraction) contents. Shale-normalized (Haskin *et al.*, 1968) REE patterns are relatively unfractionated and homogeneous throughout unit II ($(La/Yb)_n = 1.0 - 1.1$; Figure 6), in contrast with adjacent units which are more heterogeneous and variably enriched in LREE (Figure 6 and Table 1). K:Al and Th:Al variations (Figure 6) are similar to those observed for $(La:Yb)_n$. These features indicate a general congruent behaviour of large-ion lithophile elements (K, Rb, Th, La), and that the observed variations reflect source heterogeneities for detrital sedimentary inputs into the Santo André lagoon.

Geochemical indicators of palaeosalinity (Cl, Br, I, S; Chester, 1999; López-Buendía *et al.*, 1999) display characteristic concentration profiles (Figure 7), with lower values throughout subunits IA and IB and units III and IV and higher values in subunits IC to IIB. High Mg:Al values in subunits IC to IIB (Figure 7) are consistent with Cl, Br, I and S variations. All these geochemical features provide support to palaeoecological data (Cearreta *et al.*, this issue; Santos and Goñi, this issue) that indicates marine influence during deposition of subunits IC to IIB. Enhanced Cu:Pb and Zn:Pb ratios are also characteristic of subunits IC to IIB (Figure 7), suggesting non-conservative behaviour and preferential adsorption of Cu and Zn to sediment particles during seawater influx into the Santo André lagoon.

Sr isotopic compositions and $^{87}Rb:^{86}Sr$ ratio for the individual core samples are presented in Table 2. The $^{87}Sr:^{86}Sr$ and $^{87}Rb:^{86}Sr$ ratios in the analysed core samples range from 0.711157 to 0.740434 and 0.84 to 9.9, respectively. $^{87}Sr:^{86}Sr$ and $^{87}Rb:^{86}Sr$ are positively correlated ($R^2 = 0.79$) with a regressed linear slope corresponding to 219 ± 51 Ma; however, much of this correlation is due to mixing (see below), rather than radioactive decay of ^{87}Rb to ^{87}Sr, and the obtained date has no age significance (cf. Faure, 1986). Vertical variation of Sr isotopic composition of core sediments is illustrated in Figure 8 and provides important information on temporal fluctuation of source materials (e.g., Revel *et al.*, 1996; Asahara *et al.*, 1999). The $^{87}Sr:^{86}Sr$ ratio clearly discriminates between the different units/subunits, with sediments from subunits IC to IIB and IIIB being in general less radiogenic than those from subunits IA, IB, IIIA and IV (Figure 8). The higher $^{87}Sr:^{86}Sr$ values > 0.73, which predominantly reflect derivation from long-term Rb/Sr-enriched sources, correspond to subunits IB and IIIA, whereas the lower $^{87}Sr:^{86}Sr$ values < 0.715 were observed in subunits IC and IIB, reflecting the influence of less radiogenic material. In order to clarify the evolving nature of sedimentary sources and details of mixing processes, $^{87}Sr:^{86}Sr$ was plotted against Ca wt% and 1/Sr ppm^{-1} in Figure 9. Data in these figures display the characteristic trends of mixing processes (Langmuir *et al.*, 1978; Faure, 1986), indicating that the main contributions to the heterogeneity of sedimentary Sr isotopic composition were dominated by variable mixing of highly radiogenic

Table 1 Compositional data of the LSA cored sediments

Depth below surface (m)	Depth relative to m.s.l. (m)	Silt+ clay (%)	O.M.* wt%	Na wt%	Mg wt%	Al wt%	Si wt%	P wt%	S wt%	Cl wt%	K wt%	Ca wt%	Cu ppm	Zn ppm	As ppm	Br ppm	Rb ppm	Sr ppm	Sb ppm	I ppm	La ppm	Yb ppm	Pb ppm	Th ppm	U ppm
1.04–1.05	+1.69 to +1.70	77.2	1.4	0.35	1.64	7.08	29.72	0.037	0.02	0.02	2.09	2.06	43	85	15	14	106	108	1.3	nd	28.9	2.8	27	9.3	2.3
1.50–1.51	+1.23 to +1.24	55.4	0.8	0.39	1.26	5.23	34.22	0.026	0.01	nd	1.59	2.56	29	58	8.9	2.9	64	93	0.9	nd	20.0	2.0	22	5.9	1.9
1.80–1.81	+0.93 to +0.94	–	–	0.34	2.15	9.44	25.38	0.050	0.02	nd	2.95	1.41	60	108	17	5.9	156	134	1.4	nd	39.7	3.6	29	10.5	2.7
1.90–1.91	+0.83 to +0.84	99.4	1.3	0.36	2.21	9.20	25.23	0.042	0.05	nd	2.81	1.43	63	108	14	7.7	164	131	1.7	nd	41.3	3.6	29	10.8	2.8
2.27–2.28	+0.46 to +0.47	65.1	1.8	0.29	1.84	7.30	27.87	0.034	0.24	nd	2.58	2.84	43	74	12	9.1	154	135	1.2	nd	28.1	2.6	19	7.5	2.1
2.47–2.48	+0.26 to +0.27	–	–	0.07	0.11	1.40	43.69	0.007	0.07	0.01	1.06	0.35	3	5	1.3	1.5	52	30	nd	nd	5.0	0.4	11	2.2	0.8
2.84–2.85	–0.10 to –0.11	1.5	0.0	0.05	0.02	0.79	45.66	0.004	0.04	nd	0.7	0.40	2	2	0.6	nd	29	27	0.2	nd	3.5	0.2	6	1.5	0.6
3.33–3.34	–0.59 to –0.60	–	–	0.05	0.02	0.86	45.38	0.005	0.03	nd	0.82	0.05	2	2	0.5	0.8	46	13	0.2	nd	3.4	0.2	8	1.3	nd
3.70–3.71	–0.96 to –0.97	0.7	0.0	0.05	0.01	0.75	45.88	0.004	0.02	nd	0.72	0.10	2	2	nd	0.7	31	13	0.1	nd	2.8	0.2	6	1.3	nd
4.93–4.94	–2.19 to –2.20	0.7	0.0	0.04	0.03	0.78	45.74	0.005	0.01	nd	0.69	0.06	2	2	0.7	0.9	29	11	0.1	nd	3.4	0.2	6	1.3	0.6
5.43–5.44	–2.69 to –2.70	–	–	0.47	0.92	5.51	25.85	0.028	2.08	0.09	1.87	4.41	33	76	6.8	45	97	217	0.5	13	23.6	2.2	22	6.5	2.4
6.75–6.76	–4.01 to –4.02	–	–	0.48	1.22	5.99	22.40	0.033	1.87	0.14	1.94	6.01	39	80	9.4	44	107	286	0.8	11	24.4	2.3	21	6.8	2.2
7.43–7.44	–4.69 to –4.70	92.6	5.9	0.48	1.87	8.17	21.26	0.040	2.08	0.14	2.56	2.49	58	114	16	30	129	188	1.4	14	33.5	3.2	26	9.2	3.0
8.50–8.51	–5.76 to –5.77	97.6	5.5	0.55	1.74	8.04	22.10	0.044	1.59	0.20	2.41	1.32	59	125	12	39	152	133	1.1	7.4	31.6	3.1	31	9.4	2.6
10.00–10.01	–7.26 to –7.27	85.9	8.9	0.22	0.80	6.25	20.25	0.032	2.44	0.44	1.67	2.50	33	85	11	93	100	97	0.8	9.6	21.2	1.9	21	6.8	3.8
10.60–10.61	–7.86 to –7.87	74.3	6.2	0.43	2.00	7.87	21.55	0.038	1.87	0.13	2.29	3.22	52	104	11	25	114	192	1.0	6.7	30.8	2.8	24	8.4	3.0
11.10–11.11	–8.36 to –8.37	97.4	2.8	0.44	2.00	8.74	24.03	0.045	0.55	0.09	2.35	1.22	69	113	12	13	136	99	1.1	6.0	37.0	3.4	30	10.3	3.2
12.50–12.51	–9.76 to –9.77	94.0	6.9	0.42	1.88	8.41	21.51	0.047	1.24	0.16	2.37	2.18	61	112	14	53	146	142	1.3	10	31.0	3.0	23	8.8	2.4
14.09–14.11	–11.35 to –11.37	76.1	10.7	0.31	0.68	6.60	26.91	0.026	1.95	0.07	1.88	0.57	28	72	34	66	119	76	1.1	13	23.7	2.2	32	8.2	9.2
14.39–14.40	–11.65 to –11.66	79.5	8.2	0.32	1.37	7.79	22.46	0.046	1.29	0.11	2.27	1.39	43	111	12	108	145	134	1.4	14	29.7	2.6	27	9.3	3.0
14.73–14.74	–11.99 to –12.00	12.8	4.7	0.24	0.22	2.83	36.96	0.016	0.38	0.02	1.24	4.06	6	34	7.2	9.6	67	222	0.6	2.7	11.0	0.8	13	3.7	2.1
14.97–14.98	–12.23 to –12.24	14.8	5.5	0.28	0.19	2.84	40.82	0.009	0.44	0.01	1.41	0.68	6	28	3.6	3.6	67	61	0.4	nd	10.4	0.9	17	3.3	2.6
15.37–15.39	–12.63 to –12.65	76.6	9.8	0.27	0.85	7.75	25.45	0.027	1.15	0.14	2.08	0.85	32	116	23	73	128	99	1.8	16	29.3	2.8	40	9.1	8.0
16.05–16.06	–13.31 to –13.32	2.4	0.0	0.11	0.04	0.99	43.70	0.007	0.18	nd	0.86	0.04	2	8	3.5	0.7	40	16	0.3	nd	3.6	0.3	8	1.7	0.7
16.70–16.71	–13.96 to –13.97	51.9	7.3	0.33	0.64	5.89	3.45	0.030	0.80	0.04	1.75	3.02	16	76	14	36	97	177	0.8	17	22.0	2.0	28	6.5	3.2
17.30–17.31	–14.56 to –14.57	58.7	1.3	0.31	0.49	5.83	33.26	0.028	0.10	0.03	1.71	0.23	22	95	8.4	4.2	94	59	1.1	1.5	26.1	2.4	36	7.7	2.5
17.70–17.71	–14.96 to –14.97	45.6	1.9	0.25	0.46	5.36	36.50	0.009	0.10	0.04	1.72	0.16	22	78	1.5	2.3	74	55	0.8	nd	21.3	2.0	34	6.6	3.6
17.79–17.80	–15.05 to –15.06	11.6	1.9	0.17	0.11	2.23	43.16	0.005	0.12	0.01	1.11	0.02	4	12	1.3	1.1	54	27	0.2	nd	7.0	0.6	12	2.7	1.1
18.80–18.81	–16.06 to –16.07	18.3	2.7	0.16	0.11	1.80	43.14	0.007	0.13	0.02	0.99	0.49	4	17	2.9	0.9	56	38	0.3	3.6	7.2	0.5	15	2.2	1.0
19.76–19.77	–17.02 to –17.03	39.0	2.6	0.34	0.37	4.33	37.94	0.011	0.10	nd	1.88	0.19	15	53	6.1	nd	98	54	0.9	nd	20.5	1.5	29	5.4	1.6
20.24–20.26	–17.50 to –17.52	56.3	1.8	0.47	0.56	5.45	35.62	0.016	0.10	0.01	2.01	0.21	21	75	9.3	2.2	68	67	0.6	5.5	27.1	2.4	31	8.0	2.6
20.89–20.90	–18.15 to –18.16	54.0	1.6	0.33	0.50	5.38	34.32	0.025	0.23	0.02	1.69	0.43	21	89	9.8	3.2	120	64	1.1	nd	25.1	2.5	36	7.5	2.0
21.40–21.41	–18.66 to –18.67	29.5	1.1	0.25	0.30	3.48	39.60	0.011	0.04	0.01	1.55	0.12	13	43	2.9	0.8	81	42	0.7	nd	17.1	1.5	21	5.0	0.8
22.84–22.85	–20.10 to –20.11	75.8	1.0	0.62	0.59	6.49	33.10	0.017	0.12	0.01	2.21	0.24	24	81	5.8	nd	126	78	1.2	nd	38.7	3.1	40	11.2	3.1
23.60–23.61	–20.86 to –20.87	4.1	1.9	0.08	0.04	1.09	44.81	0.012	nd	0.01	0.8	0.02	2	7	0.9	nd	38	16	0.2	nd	5.1	0.4	11	2.0	0.7

*Relative to silt+clay fraction; – not determined; nd under detection limit.

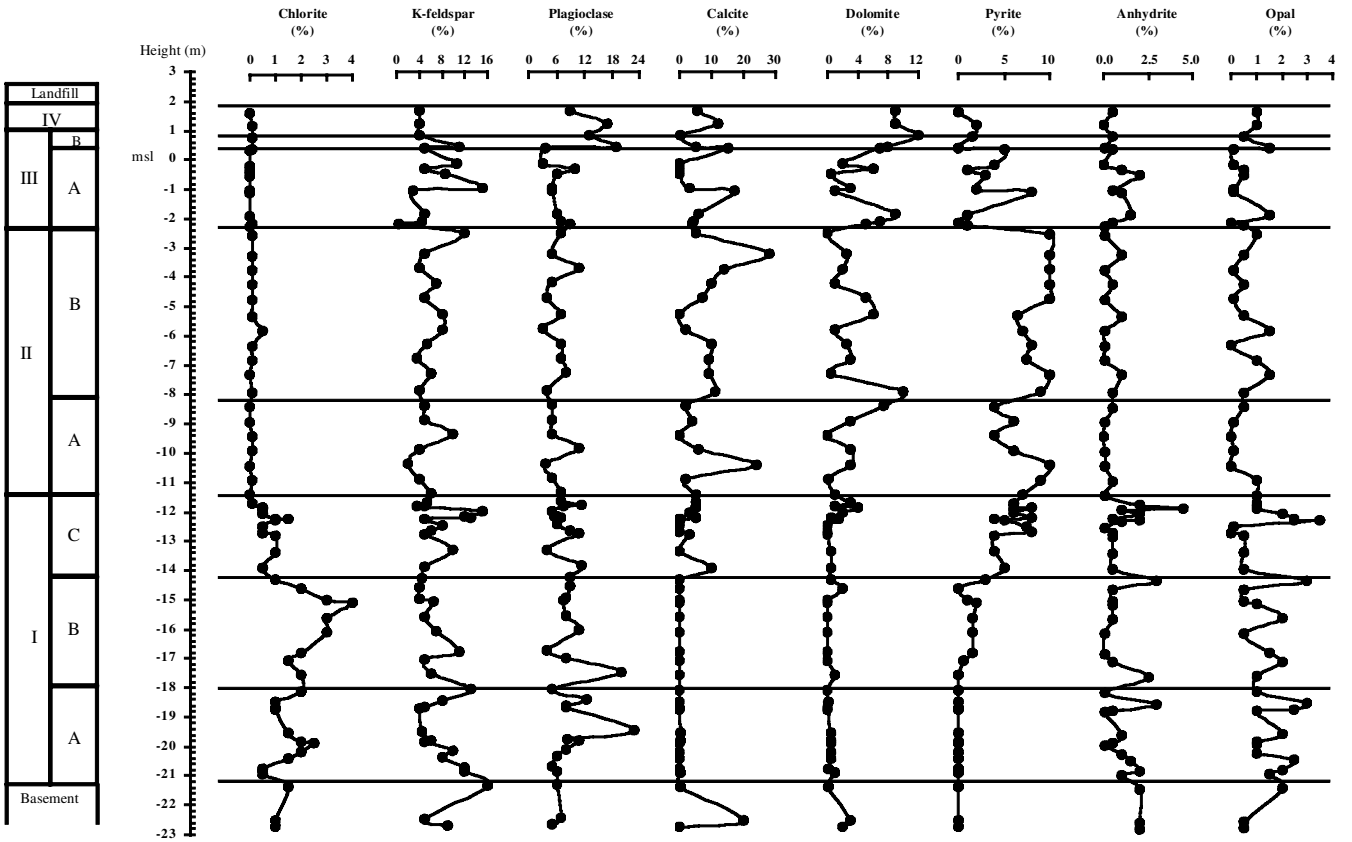

Figure 4 Vertical concentration profiles of selected minerals in the <63 μm fraction.

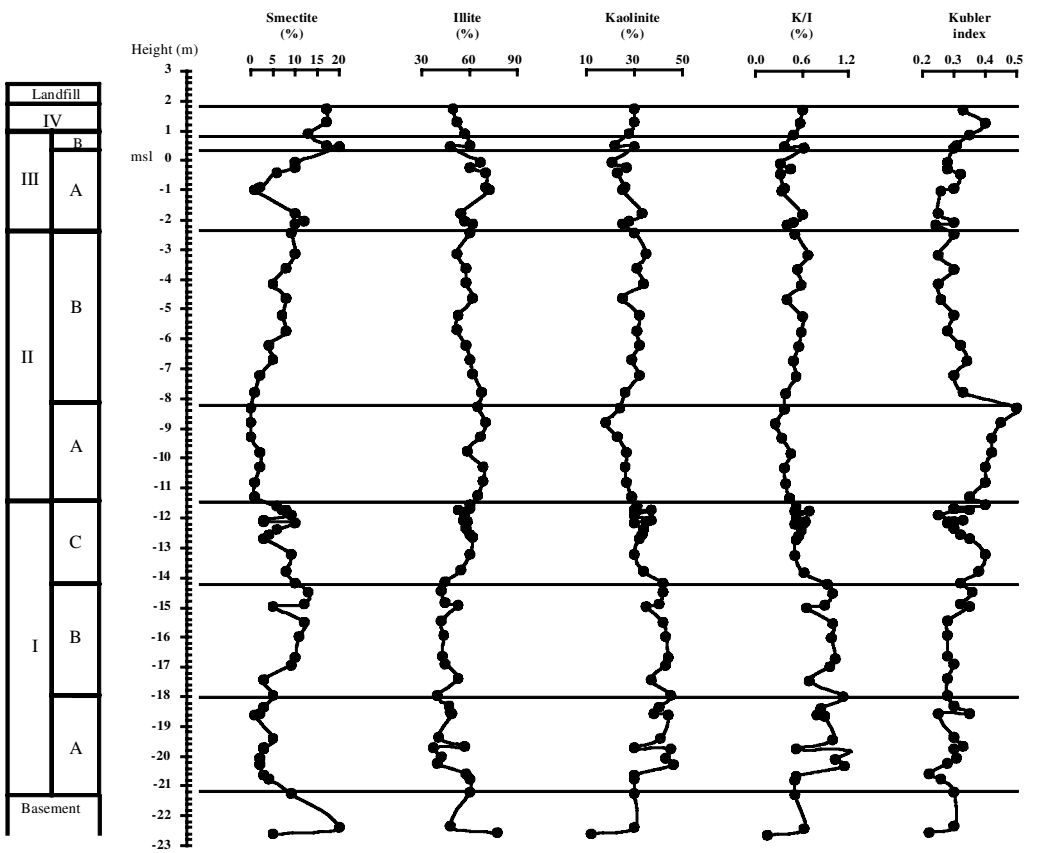

Figure 5 Vertical concentration profiles of selected clay minerals, K:I ratio and Kubler's crystallinity index in the <2 μm fraction.

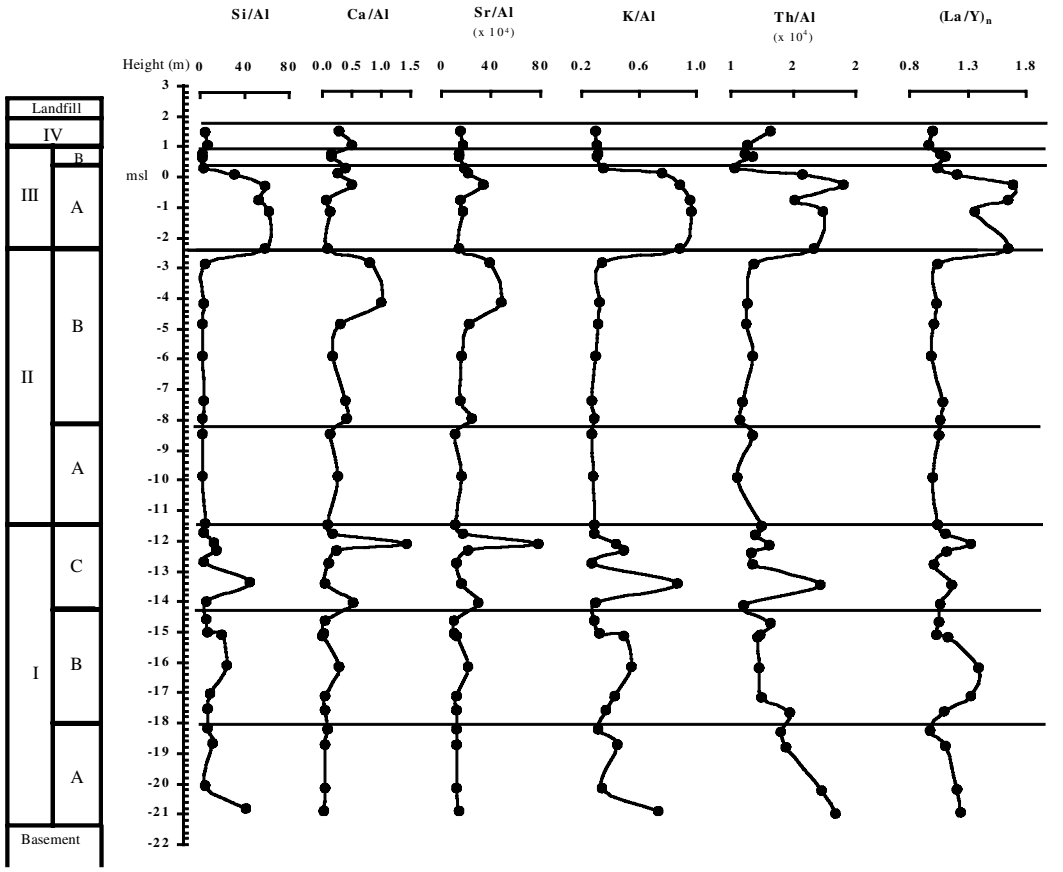

Figure 6 Vertical profiles of selected elemental ratios dependent on lithological and textural attributes (subscript $_n$ indicates normalized values).

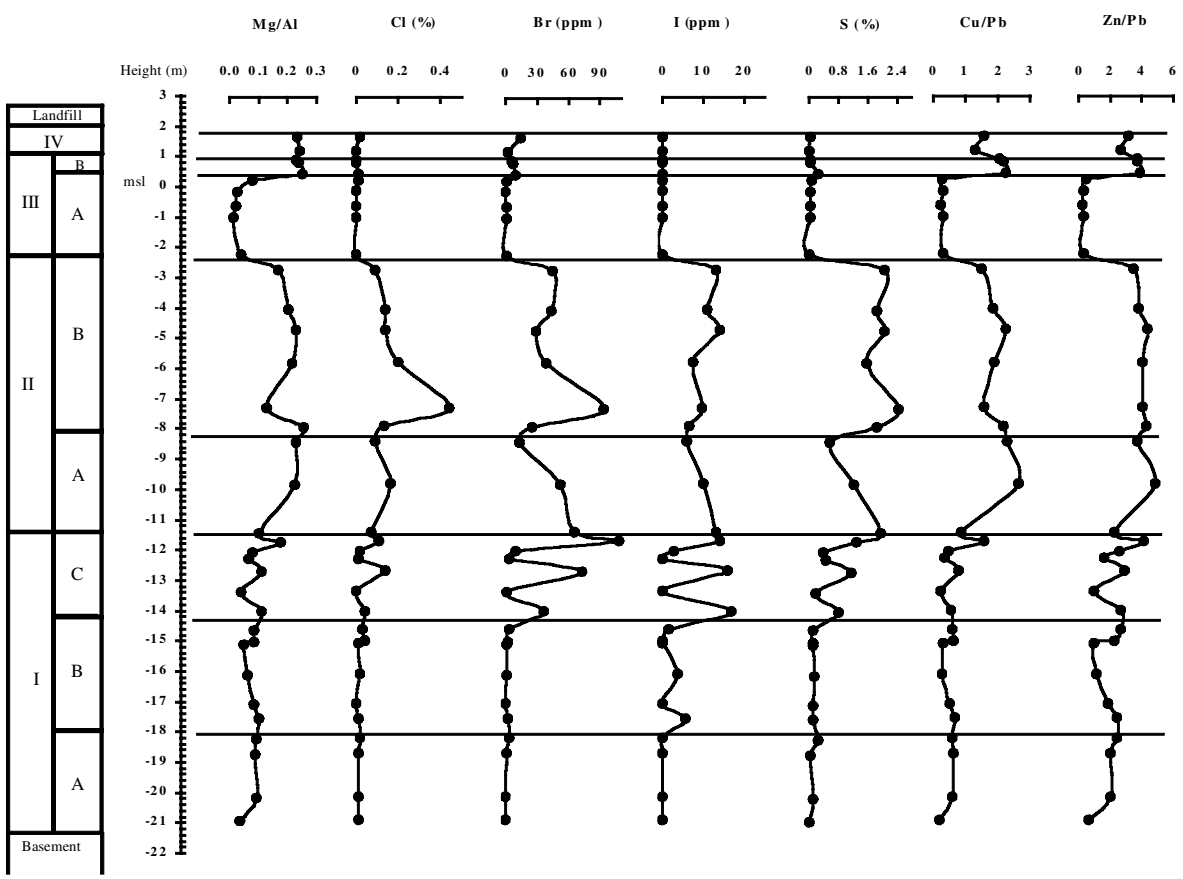

Figure 7 Vertical profiles of selected elemental concentrations/ratios indicative of variable marine/terrestrial inputs.

Table 2 $^{87}Sr:^{86}Sr$ and $^{87}Rb:^{86}Sr$ isotopic ratios of samples from core LSA

Depth relative to m.s.l. (m)	Depth below surface (m)	Unit/subunit	$^{87}Sr:^{86}Sr$	Error (2σ)	$^{87}Rb:^{86}Sr$
+0.93 to +0.94	1.80 to 1.81	IV	0.719293	0.000027	3.262
+0.83 to +0.84	1.90 to 1.91		0.719240	0.000072	3.508
+0.46 to +0.47	2.27 to 2.28	IIIB	0.717663	0.000022	3.196
+0.26 to +0.27	2.47 to 2.48		0.724226	0.000029	4.859
–0.10 to –0.11	2.84 to 2.85	IIIA	0.726312	0.000051	3.011
–0.59 to –0.60	3.33 to 3.34		0.740434	0.000054	9.931
–2.69 to –2.70	5.43 to 5.44		0.712717	0.000057	1.252
–4.01 to –4.02	6.75 to 6.76		0.712631	0.000040	1.047
–4.69 to –4.70	7.43 to 7.44	IIB	0.714732	0.000036	1.922
–7.26 to –7.27	10.00 to 10.01		0.716421	0.000086	2.888
–7.86 to –7.87	10.60 to 10.61		0.715482	0.00005	1.663
–8.36 to –8.37	11.10 to 11.11		0.716281	0.000029	3.848
–9.76 to –9.77	12.50 to 12.51	IIA	0.716536	0.000039	2.880
–11.35 to –11.37	14.09 to 14.11		0.722999	0.000058	4.389
–11.65 to –11.66	14.39 to 14.40		0.718622	0.000036	3.032
–11.99 to –12.00	14.73 to 14.74		0.711157	0.000040	0.845
–12.23 to –12.24	14.97 to 14.98	IC	0.721634	0.000022	3.078
–12.63 to –12.65	15.37 to 15.39		0.715878	0.000021	3.621
–13.96 to –13.97	16.70 to 16.71		0.715102	0.000053	1.535
–14.56 to –14.57	17.30 to 17.31		0.723418	0.000029	4.466
–15.05 to –15.06	17.79 to 17.80	IB	0.73247	0.000011	5.611
–17.50 to –17.52	20.24 to 20.26		0.725554	0.000015	2.845
–18.15 to –18.16	20.89 to 20.90		0.722847	0.000072	5.255
–20.10 to –20.11	22.84 to 22.85	IA	0.724493	0.000051	4.528

(low-Ca, Sr), terrigenous, clay material with relatively unradiogenic, (high-Ca, Sr), carbonates. Even at low Ca contents (equivalent to <20% of $CaCO_3$; Figure 9A), the carbonate fraction dominates the isotopic composition and concentration of Sr in the sediments. Regression of data points in Figure 9B define two straight lines with distinct slopes for subunits IA, IB, IIIA, IV and subunits IC, IIA, IIB, IIIB, respectively; these features suggest the operation of more than two end-member components in the mixing process. Mixing calculations for subunit IC, IIA, IIB and IIIB samples (Figure 9B) indicate that their isotopic compositions and Sr concentrations comply with the involvement of a seawater-derived carbonate end-member component ($^{87}Sr:^{86}Sr = 0.7092$, Sr ~ 2000 ppm; Burke *et al.*, 1982), which is consistent with the remaining geochemical evidence (Figure 7). On the other hand, extrapolation of the regression line for subunits IA, IB, IIIA and IV to $1/Sr = 0$ requires a carbonate component in these sediments with $^{87}Sr:\ ^{86}Sr \sim 0.718$ (Figure 9B), implying derivation from a much more radiogenic source than that of modern marine carbonates. It thus seems that carbonate precipitating during deposition of subunits IA, IB, IIIA and IV acquired Sr from waters with quite higher $^{87}Sr:^{86}Sr$ than those contemporaneous with the deposition of subunits IC, IIA, IIB and IIIB. The former were predominantly riverine waters, deriving their radiogenic Sr from drainage of continental rocks, whereas the latter represent variable mixtures of these waters with less radiogenic seawater fluxes into the lagoon. Together with the highly radiogenic Sr that was carried in river water terrigeneous (particulate) matter, these two major sources of Sr (cf. Martin and Maybeck, 1979) should account for the Santo André lagoon sedimentary isotopic budget. Thus, isotopic heterogeneity of sediments in subunits IA, IB, IIIA and IV (Figure 8) reflect variations on the relative Sr contents of suspended and dissolved loads in the fluvial input; surely, the higher $^{87}Sr:^{86}Sr$ values in subunits IB (0.73247/–15.05 m) and IIIA (0.740434/–0.59 m) correspond to a large predominance of terrigeneous sedimentation at these times. In contrast, sediments from subunits IC, IIA, IIB and IIIB all seem to have included a significant proportion of seawater-derived Sr component. The lowest $^{87}Sr:^{86}Sr$ value (0.711157/–11.99 m), close to the top of subunit IC (Figure 8), corresponds to an inversion on the isotopic evolutionary trend, denoting an increased influence of continental sedimentation or, more probably, a decrease of seawater-derived Sr input into the lagoon; nevertheless, some seawater influx seems to have been sustained throughout most of unit II, reappearing transiently in subunit IIIB (Figure 8).

The changing sedimentation regime at the transition between subunits IC and IIA is coincident with a striking enrichment of geochemical indicators of productivity conditions (P, As, Sb, U; Figure 10), which is consistent with a concomitant enhanced production of organic matter (Figure 2). The congruent behaviour of all indicators strongly suggests that the Santo André lagoon has developed an optimum environment for biological activity at these times.

Radiocarbon dating and sedimentation rates

Dating results obtained from the LSA and exploration cores are summarized in Tables 3 and 4, and Figure 11. Datings are in stratigraphical order and four samples fall within the interval for which calendar calibration is not possible. Error bars corresponding to both the $\pm 1\sigma$ age-deviation and absolute elevation error of each dated sample are contained within the geometric dot that represents each sample in Figure 11.

Fine-grained (specially organic and clay-rich) sediments usu-

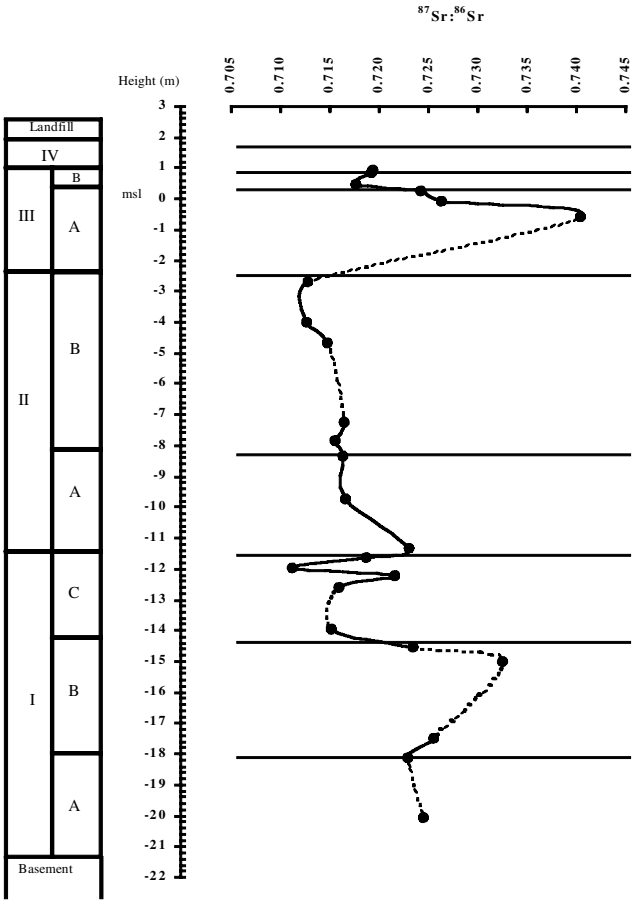

Figure 8 Vertical profile of $^{87}Sr:^{86}Sr$ ratio.

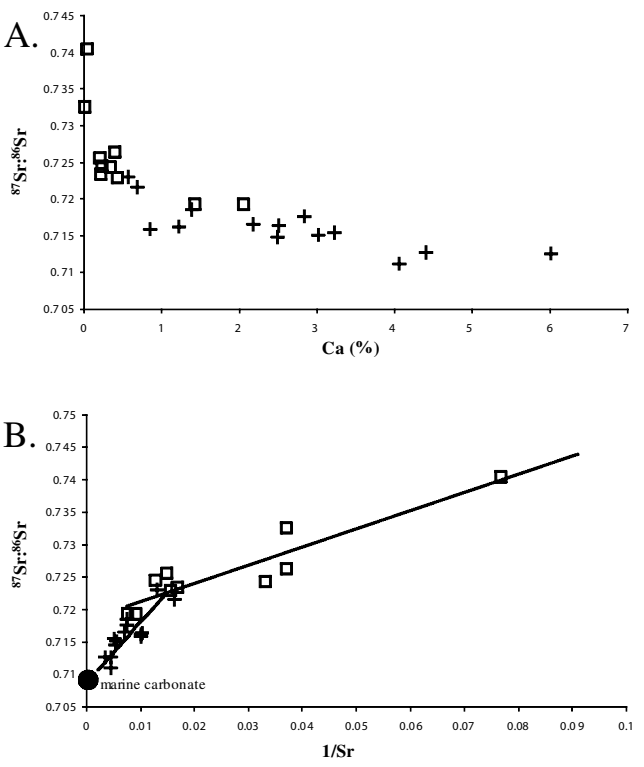

Figure 9 (A) Plot of $^{87}Sr:^{86}Sr$ versus Ca. (B) Plot of $^{87}Sr:^{86}Sr$ versus 1/Sr. Solid lines represent mixing (see text). Open squares: samples from subunits IA, IB, IIIA and unit IV. Crosses: samples from subunits IC, IIA, IIB and IIIB.

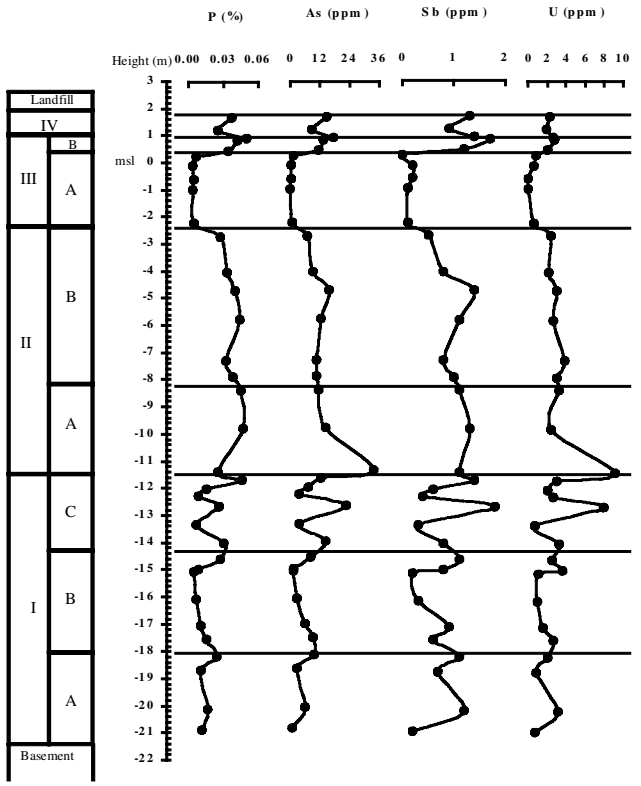

Figure 10 Vertical concentration profiles of selected elements (productivity indicators).

ally suffer postdepositional compression, which affects bed thickness and may change the elevations of sample positions and reference horizons. The basement and units I, III and IV consist essentially of coarse clastic sediments (Figure 2) which are virtually incompressible. The few interbedded muddy layers found within the different units are thin, contained between permeable boundaries and laterally unconfined, suggesting that any effect of volume reduction associated with expulsion of pore fluid should have taken place shortly after deposition. In consequence, the elevations of reference samples below –12.65 m may be considered unchanged in what post-depositional compression is concerned. This assumption is supported by the downcore profile of bulk dry density which reflects the major textural contrasts and remains virtually independent of depth.

In contrast, sediments of unit II are essentially muddy and contain a non-negligible amount of O.M. The changes in elevation of each reference sample considered within this unit and resulting from consolidation were evaluated solving Terzaghi's compression law in order to height, following Paul and Barras (1998). The sample Beta 121075 is located close to the boundary with the underlying incompressible unit and this accounts for a negligible compression effect, estimated at 1–2 cm. Samples Beta 134568 and Beta 121074 are virtually indistinguishable in terms of age and might have been displaced by 30–40 cm in relation to their original elevation due to consolidation. These effects translate into reduced impacts in the estimated net sedimentation rates, which could increase by 0.2 mm yr^{-1} relative to the figures presented below.

The resulting age-depth profile (AMS radiocarbon age model) from core LSA (Figure 11) suggests three different periods in what concerns net sedimentation rates, estimated using linear regression. From the base of the core until 10 ka an average rate of 1.34 mm yr^{-1} was found. Between 10 ka and *c*. 5.4 ka this figure dropped by one order of magnitude, averaging 0.61 mm yr^{-1}. After 5.4 ka until present, the sedimentation rate reaches an average of 2.52 mm yr^{-1}, the maximum value observed in this

Table 3 Radiocarbon dates from core LSA

Lab. code	Depth relative to m.s.l. (m)	Depth below surface (m)	$\delta^{13}C$ (‰)	Date (^{14}C years BP $\pm 1\sigma$)	Calibrated age (1σ calibrated results)
Beta-121073	–2.54–2.55	5.28–5.29	–25.9	1620 ± 40	Cal. AD 430 (cal. AD 410–465 and 475–515)
Beta-121074	–7.22–7.23	9.96–9.97	–24.8	3570 ± 50	Cal. BC 1900 (cal. BC 1955–1875 and 1805–1795)
Beta-134568	–8.16–8.17	10.90–10.91	–23.4	3570 ± 50	Cal. BC 1910 (cal. BC 1965–1880)
Beta-121075*	–11.66–11.67	14.40–14.41	–28.1	5380 ± 50	Cal. BC 4240 (cal. BC 4320–4215 and 4185–4160)
Beta-121076	–12.65–12.66	15.39–15.40	–26.1	7210 ± 50	Cal. BC 6005 (cal. BC 6045–5980)
Beta-121077	–14.49–14.50	17.23–17.24	–29.7	10020 ± 50	–
Beta-121078	–18.44–18.45	21.18–21.19	–29.6	12440 ± 50	–
Beta-121079	–19.84–19.85	22.58–22.59	–28.7	14020 ± 60	–
Beta-121080	–20.16–20.17	22.90–22.91	–29.2	14160 ± 60	–

*Wood.

Table 4 Radiocarbon dates from exploration cores

Lab. code	Depth relative to m.s.l. (m)	Depth below surface (m)	$\delta^{13}C$ (‰)	Date (^{14}C years BP $\pm 1\sigma$)	Calibrated age (1σ calibrated results)
Beta-117144*	–1.24–1.25	2.64–2.65	–27.9	160 ± 40	Cal. AD 1680 to 1935
Beta-117145	–6.30–6.32	7.30–7.32	–24.6	2150 ± 40	Cal. BC 180 (cal. BC 200 to 115)
Beta-117146	–6.73–6.75	8.83–8.85	–25.2	3580 ± 50	Cal. BC 1910 (cal. BC 1965 to 1880)

*Wood.

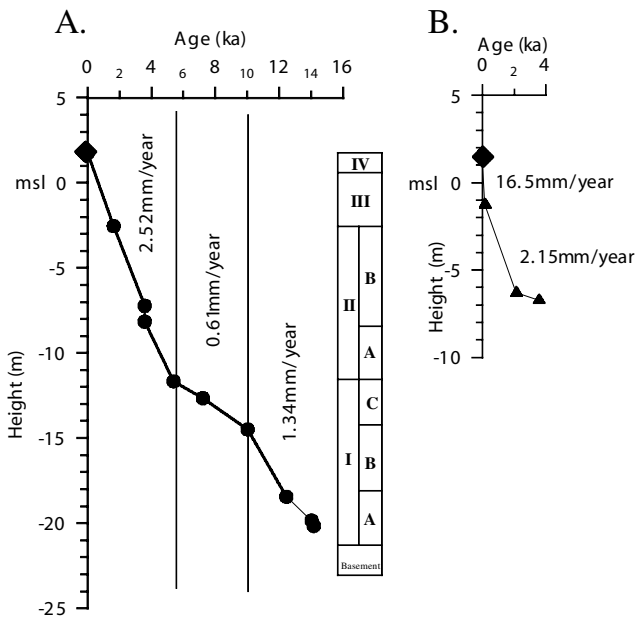

Figure 11 Age model of LSA borehole (A) and exploration cores (B). Black diamonds: present-day surface sample.

sequence, doubling the rate found in its lower section. This figure was used to interpolate an estimated age of *c*. 350 BP for the top of unit III.

Results obtained from the exploration cores, although scarce, provide useful information (Figure 11B). The average net sedimentation rate during the last 3.5 ky matches the figures found in the upper section of core LSA. However, the sediment column accumulated since 160 ± 40 BP (Table 4) corresponds to a present-day sedimentation rate of 16.5 mm yr^{-1}, a figure that increases by one order of magnitude the highest long-term average rate found along the whole sequence.

Discussion and palaeoenvironmental interpretation

In borehole LSA distinctive units and subunits can be distinguished, showing contrasts in their textural and compositional attributes, which reflect the general environmental evolution of this lowland since the Lateglacial. In general, boundaries separating lithostratigraphical units are equivalent in the different textural, mineralogical, geochemical and palaeontological properties.

Subunits IA (14160 ± 60 to 12440 ± 60 BP) and IB (12440 ± 60 to 10020 ± 50 BP)

These subunits record a sedimentation of alternating low and high energy, the latter episodes corresponding to coarse clastic poorly sorted material; the presence of muscovite, fermented plant remains and charcoal, together with slate pebbles within both the coarse and fine-grained layers suggests a terrestrial sedimentation environment and a proximal sediment source. The geochemical proxies confirm a terrestrial sedimentation environment: the contents of marine-borne elements (Cl, Br, I and S) are consistently very low, and source-sensitive lithophile element ratios agree with a continental provenance: La:Yb, Th:Al and K:Al are high, whereas Mg:Al, Cu:Pb and Zn:Pb are low. In addition, the high ^{87}Sr:^{86}Sr values clearly indicate a terrestrial environment. In subunit IA the abundance of detrital minerals in the <63 μm fraction and of kaolinite in the clayey fraction also suggest a terrestrial sedimentation environment and intensive weathering in the source area. The presence of chlorite may indicate a high erosion rate of the topsoil, exceeding the rates of hydrolysis of the substrate. Transition to subunit IB is possibly marked by a morphoclimatic

change with increasing semi-arid conditions but also some maturation of the fluvial network: flood plains were possibly present, favouring the development of Smectite. Subunits IA and B represent terrestrial sedimentation in fluviatile environment contemporaneous of a low sea level and a distal shoreline. This is confirmed by the complete absence of foraminifera, representative ostracoda, calcareous nannoplankton and diatoms in subunit IA and the scarcity of foraminiferal tests, absence of both representative ostracods and coccoliths in subunit IB (cf. Cearreta *et al.*, this issue). They correspond to the Bölling-Allerød Interstadial and include both the upper sections of the Older Dryas and the Younger Dryas. At this time, the Santo André area was located in a lowland, incised in Miocene basement that extended westwards through a wide coastal plain. Regarding mean sea level our data only indicate that marine influence remain below –14 m during this period.

Subunit IC (10020 ± 50 to 5380 ± 50 BP)

This subunit is characterized by a decrease in the slope of the best-fit regression line in the age model (Figure 11). In general, no significant textural contrast is noticeable in comparison with subunit IB. However, different sedimentation episodes can be distinguished within this subunit using bioclastic and O.M., mineralogical and geochemical signatures. Indeed, values of these attributes oscillate in a synchronous way along this subunit and the positive and negative variations are coherent in their environmental significance: the very base of the subunit (–14.26 to –13.50 m) show high contents of marine borne elements (I, Br, S), bioclasts and O.M., as well as high Mg:Al, Ca:Al and Sr:Al ratios and low K:Al, Th:Al values. This signature is repeated between –12.70 and –12.50 m and above –12.22 m. In between (–13.50 to –12.70 m and –12.50 to –12.22 m) two horizons exhibit elemental ratios and contents that perform an opposite behaviour, suggesting episodes of terrestrial influence. The available ^{87}Sr:^{86}Sr data is consistent with this oscillating sedimentary regime, supporting a strong marine influence during deposition of this subunit. Transition from subunit IB to IC is marked by an increase of the Mg:Al ratio, suggesting additional inputs of Mg from seawater. Cu:Pb and Zn:Pb ratios are quite variable along this subunit and exhibit a general upward increasing trend. In the upper half of this subunit positive and negative oscillations of these ratios perfectly match the variations observed in seawater-enriched halogen elements, a feature that is not so evident in its lower half. The relative increment of illite in the clay mineral assemblages also suggests an increasing marine influence in this subunit; in its upper section the content in pyrite and opal C/CT suggests a progressively more restricted environment.

Subunit IC essentially represents sedimentation in an open marine environment, disturbed by two episodes of continental sedimentation; its lower boundary corresponds to a sea-level marker. According to Cearreta *et al.* (this issue) it yielded an abundant and diverse foraminiferal assemblage with a mixture of hyaline and porcellaneous species (dominated by *Ammonia beccarii*, *Haynesina germanica* and *Quinqueloculina seminula*), an ostracod assemblage of marine littoral or sublittoral species of moderate diversity (dominated by *Loxoconcha rhomboidea, Aurila convexa, Aurila arborescens, Carinocythereis whitei, Urocythereis britannica, Pontocythere elongata, Pontocythere* cf. *trigonella*) and an association of almost exclusively marine planktonic diatoms. The Santo André area would have been an open gulf environment where the proximity of the terrestrial margin allowed temporary fluvial incursions due to minor sea-level oscillations or massive fluvial solid discharges.

Subunits IIA and IIB (5380 ± 50 to 1620 ± 40 BP)

These subunits exhibit a dramatic textural contrast in comparison with unit I: the abundance of the >63 μm fraction drops whereas bioclasts and O.M. contents increase. The average net sedimentation rate increases one order of magnitude (averaging 2.6 mm yr^{-1}).

Subunit IIA (5380 ± 50 to 3570 ± 50 BP)

This subunit is extremely uniform in texture, being compatible with a low-energy restricted sedimentation environment where continuous deposition of cohesive sediment together with particulate organic matter defined propitious conditions for the settlement of carbonate-shelled bivalves, such as *Cerastoderma edule*, whose remnants are frequently preserved as whole shells in the sediment. Si:Al values indicate predominance of clay minerals in the fine fraction. Marine geochemical proxies vary upwards in this subunit suggesting decreasing marine influence, which is however still more important than in subunits IA and IB. ^{87}Sr:^{86}Sr values rapidly increase at the boundary between subunits IC and IIA, suggesting development of severe restrictions to major seawater flux into the lagoon at this time; however, the ^{87}Sr:^{86}Sr ratio remains sufficiently low to be consistent with marine influence on the deposition of subunit IIA. The exclusive presence of the diatom *Paralia sulcata* at this boundary should be an indication of this isolation event. The increase in carbonates (especially calcite), pyrite and illite in the mineralogical assemblages of both the fine and clayey fractions indicates a restricted environment.

Subunit IIB (3570 ± 50 to 1620 ± 40 BP)

This subunit shows small variations of the relative abundance of the <63 μm fraction, which correlates with abundance maxima of both the Ca carbonate content and the Ca:Al and Sr:Al ratios; Si:Al ratio remains low and quite uniform throughout this subunit. This suggests a continuity of the background low-energy sedimentation punctuated by lag deposition of bioclasts. Geochemical signatures of I, Cl, Br, S and Mg:Al indicate a well-defined episode of marine influence in the lower half of this subunit (peak values at *c.* –7.3 m); this episode is followed by a trend of decreasing ^{87}Sr:^{86}Sr values, confirming a significant seawater input into the lagoon. In its upper half, the same elemental contents are similar to those found in subunit IIA. Transition from subunits IIA to IIB translates into a reversal of the variation trend of the K:I ratio which is synchronous with a decrease of the Kubler crystallinity index of illite, indicating the input of significant amounts of degraded illite, probably due to an increase of pluviosity in the source areas. The abundance of pyrite and calcite in the fine fraction indicates persistence of confined environmental conditions.

Unit II represents low-energy sedimentation in a restricted environment. The Santo André area became a coastal lagoon in consequence of the development of an efficient detrital barrier *c.* 5400 BP which translated into the geological record as the sharp lower boundary of subunit IIA. Unit II sedimentological signatures reflect the distal location of the borehole in relation to the barrier and, above all, the changes on the efficiency of the barrier structure, both as a hydrodynamic filter and as an isolation/connection element of the lagoonal space in relation with the ocean through the tidal inlet and overwash. Actually, subunit IIA corresponds to a period of higher efficiency of the barrier: water exchange with ocean through the inlet was negligible but overwash would exist. Sediment input was essentially of terrestrial provenance, added by *in situ* inputs of O.M. and carbonate shells. This facies may be found in the present day analogues in the deepest and central areas of Santo André and other Portuguese coastal lagoons during closed inlet episodes. This interpretation is corroborated by the very low foraminiferal and ostracod abundance, which indicate modal fresh to slightly brackish water conditions punctuated by occasional marine inputs (overwash), expressed by the coccolith content (Cearreta *et al.*, this issue). Subunit IIB reflects a more permeable barrier (illustrated by an abundant, low-diverse, pyritized foraminiferal assemblage, domi-

nated by *H. germanica*, *A. beccarii* and *Elphidium oceanensis*, and by a very abundant, low-diversity ostracod assemblage, highly dominated by *Cyprideis torosa*) possibly due to a more frequent breaching of the barrier and/or permanency of an inlet that changed the modal conditions to an essentially brackish environment.

Subunits IIIA and IIIB (1620 ± 40 to c. 350 BP)

These subunits are quite different in their sedimentological and geochemical characteristics. In the lower subunit the sedimentation environment resumes high-energy conditions and terrigenous source indicated by coarse clastic texture, low bioclastic and O.M. contributions to the total sample. Elemental and isotopic geochemical proxies clearly support terrestrial sources/inputs. This is corroborated by the decrease of the K:I ratio and reappearance of smectite. In what concerns palaeoecological content, the lower subunit is barren of coccoliths and contains low foraminiferal and ostracod abundances (Cearreta *et al.*, this issue). The top subunit is exceptional because it represents a short-lived return to a brackish, low-energy environment; this episode is well characterized by a marked decrease of the ^{87}Sr:^{86}Sr ratio and was accompanied by an increase in productivity with expression in total O.M. and bioclasts. Evaporation of ponded water may be responsible for the predominantly dolomitic nature of the carbonated minerals present in the fine-grained fraction. Unit III represents marginal lagoonal sedimentation under fresh to brackish water conditions and almost exclusively fed by terrestrial sediment inputs. It corresponds to the late stages of silting up of the lagoonal basin in the coring area, involving expansion of the prograding alluvial plain over the lagoon.

Unit IV (c. 350 BP to present day)

This unit was sedimented in a low energy terrigenous environment (coarser particles are partly of biogenic nature), as suggested by textural signature, low O.M. content, low Si:Al ratio and palaeoecological signature: it is barren of any foraminifera, representative ostracoda, calcareous nannoplankton and diatoms (Cearreta *et al.*, this issue). The clay fractions show an increase in kaolinite followed by an increase in smectite, suggesting a regressive pattern of the sedimentary conditions. Cl, I, Br and S contents are similar to those of subunit IIIA, whereas ^{87}Sr:^{86}Sr are lower reflecting a stronger influence of carbonate to the Sr sedimentary budget. The high values of Zn:Pb and Cu:Pb found in the uppermost section of this unit (reversing the upward decreasing trend of its lower section) might be a consequence of anthropogenic activity. Unit IV represents the present-day sedimentation environment at the coring site: an accreting alluvial plain relatively distal of the main channel, flooded during the rainy season where sediment laminae are disturbed by bioturbation. The topmost 1 m of landfill corresponds to a real estate limit and simultaneously to a small dyke to control flooding of grazing land.

Conclusions

The sedimentological and geochemical study of the LSA borehole, that represents the infill of a sector of the Santo André coastal lowland during the last 14 ka, allows the reconstruction of the environmental changes that occurred in this area during this period that translated into contrasting lithostratigraphical units. The pre-Holocene section of the core represents terrestrial sedimentation in a fluviatile environment, contemporaneous of a low sea level and a distal shoreline. Sediment inputs were terrestrial and resulting from intensive weathering and high erosion rate in the adjacent watershed. During the early Holocene (*c.* 10020 to 5380 BP), the eustatic forcing factor determined coastal changes: the sea invaded this lowland and defined an open marine shallow environment corresponding to a wide gulf which has been disturbed by distinct (and apparently distal) terrestrial inputs. The base of subunit IC is a clear sea-level marker, whereas the facies changes observed in this subunit may have been induced by massive episodes of fluvial discharge. To the top, the first symptoms of confinement have been noted, suggesting that incipient barriers may have formed. *C.* 5380 BP, a major environmental threshold is recorded by the establishment of an efficient detrital barrier that completely isolated the previous open bay and changed this area to a closed coastal lagoon. The development of this barrier is most probably an effect of the marked deceleration of the sea-level rise rate that took place at this time. After 5380 BP, the lagoonal environment evolved essentially as a function of local forcing factors, among which the frequency and efficiency of exchanges with the ocean (promoted by overwash and mainly by a tidal inlet) were the more important. Until *c.* 3570 BP the lagoonal environment was quite restricted, dominated by freshwater inputs and terrestrial sediments added by a significant production of organic matter that promoted rapid silting up of the basin. A second episode of lagoonal sedimentation lasts until *c.* 1620 BP reflecting brackish conditions and increased marine influence due to a decrease of the efficiency of the barrier. The upper units III and IV represent final stages of filling of the lagoonal margin by fluvial activity including the progradation of the alluvial fans. Human intervention in the breaching of this barrier is documented since the seventeenth century and in similar environments of the Portuguese coast since the fifteenth century, but it is highly probable that this procedure might have started earlier. This is a plausible cause of the short-lived return to brackish conditions recorded at subunit IIIB which later fade away due to the inner location of the coring site that allowed fluvial facies to take over.

This study indicates that downcore geochemical variations on Al, Ca and Sr primarily reflect lithological/textural heterogeneity whereas several elemental/isotopic contents/ratios (namely Cl, Br, I, S, Mg:Al, Cu:Pb, Zn:Pb, Th:Al, K:Al and ^{87}Sr:^{86}Sr) correlate with variable sediment sources and relative importance of marine/terrestrial inputs to the coastal basin. This statement demonstrates the significance of the geochemistry as an environmentally sensitive proxy of coastal changes.

Acknowledgements

This paper is a contribution to the Research Projects PRAXIS/PCNA/T/CTE/12/96 'Holocenic evolution of the SW Portuguese coast' and PRAXIS/PDCTM/P/MAR/ 15231/1999 'Global versus Local Forcing Factors and Palaeoenvironmental Changes of Estuaries and Lagoons of SW Portugal Since the Lateglacial' financed by the Portuguese FCT (Fundação para a Ciência e Tecnologia).

References

Asahara, Y., Tanaka, T., Kamioka, H., Nishimura, A. and **Yamazaki, T.** 1999: Provenance of the north Pacific sediments and process of source material transport as derived from Rb-Sr isotopic systematics. *Chemical Geology* 158, 271–91.

Bao, R., Freitas, M.C. and **Andrade, C.** 1999: Separating eustatic from local environmental effects: a late-Holocene record of coastal change in Albufeira lagoon, Portugal. *The Holocene* 9, 341–52.

Burke, W.H., Denison, R.E., Hetherington, E.A., Koepnick, R.B., Nelson, N.F. and **Otto, J.B.** 1982: Variation of seawater $^{87}Sr/^{86}Sr$ throughout Phanerozoic time. *Geology* 10, 516–19.

Cardoso, L. 1747: *Diccionario geografico ou noticia historica*, volume 1. Lisboa: Regia Officina Sylviana e Academia Real, 756 pp.

Chester, R. 1999: *Marine geochemistry*. Oxford: Blackwell Science, 506 pp.

Clark, J.A., Farrell, W.E. and **Peltier, W.R.** 1978: Global changes in postglacial sea level: a numerical calculation. *Quaternary Research* 9, 265–87.

Dias, J.M.A. 1985: Registos da migração da linha de costa nos últimos 18000 anos na plataforma continental Portuguesa setentrional. *Actas I Reunião Quaternário Ibérico* I, 281–95.

—— 1987: Dinâmica sedimentar e evolução recente da plataforma continental Portuguesa setentrional. Unpublished PhD dissertation, Departamento de Geologia, Universidade de Lisboa, 471 pp (available from author).

Faure, G. 1986: *Principles of isotope geochemistry*. Chichester: Wiley, 589 pp.

Folk, R.L. 1974: Petrology of sedimentary rocks. Austin, Texas: Hemphill Publishing Co., 184 pp.

Freitas, M.C. 1995: A Laguna de Albufeira (Península de Setiuúbal). Sedimentologia, Morfologia e Morfodinâmica. Unpublished PhD thesis, Departamento de Geologia, Universidade de Lisboa, 337 pp (available from author).

Freitas, M.C. and **Andrade, C.** 1994: Tidal inlet evolution and hydraulic characteristics at Albufeira Lagoon. *Proceedings LITTORAL'94*, 257–71.

Freitas, M.C., Andrade, C. and **Romariz, C.** 1993: *Middle and late Holocenic evolution of the Melides barrier (SW Portugal). First results*. Strasbourg: Terra Abstracts, EUG VII, 613–14.

Friedman, G. and **Sanders, J.** 1978: *Principles of sedimentology*. Chichester: Wiley, 792 pp.

Haskin, L.A., Haskin, M.A., Frey, F.A. and **Wildeman, T.R.** 1968: Relative and absolute terrestrial abundances of the rare earths. In Ahrens, L.H., editor, *Origin and istribution of the elements*, Oxford: Pergamon, 889–911.

Hayes, M.O. 1978: Barrier island morphology as a function of tide and wave regime. In Leatherman, S.P. editor, *Barrier islands. From the Gulf of St Lawrence to the Gulf of Mexico*, London: Academic Press, 1–29.

Kawachita, K. 1972: O método Rb/Sr em rochas sedimentares. Aplicação para as Bacias do Paraná e Amazonas. Unpublished PhD thesis, Instituto Geociências, University of São Paulo (Brasil), 111 pp (available from author).

Kubler, B. 1964: Les argiles, indicateurs de métamorphisme. *Revue Institut Français de Pétrole* 19, 1093–112.

Langmuir, C.H., Voke, R.D. Jr, Hanson, G.N. and **Hart, S.R.** 1978: A general mixing equation with applications to Icelandic basalts. *Earth Planetary Science Letters* 37, 380–92.

Larsonneur, C. 1977: La cartographie des dêpots meubles sur le plateau continental français: méthode mise au point et utilisée en Manche. *Journal Recherche Oceanographique* 2(2), 33–39.

LNEC 1967: *Solos – determinação do teor em matéria orgânica*. Especificação LNEC E-201, Lisboa: Laboratório Nacional de Engenharia Civil, 3 pp.

López-Buendía, A.M., Bastida, J., Querol, X. and **Whateley, M.K.G.** 1999: Geochemical data as indicators of paleosalinity in coastal organic-rich sediments. *Chemical Geology* 157, 235–54.

Martin, J.M. and **Maybeck, M.** 1979: Elemental mass balance of material carried by major world rivers. *Marine Chemistry* 7, 173–206.

Mateus, J. 1992: Holocene and present-day ecosystems of the Carvalhal region, Southwest Portugal. PhD dissertation, University of Utrecht, 184 pp.

Nichols, M. and **Allen, G.** 1981: Sedimentary processes in coastal lagoons. Proceedings of Coastal Lagoon Research, Present and Future. *UNESCO Technical Papers in Marine Science* 33, 27–80.

Paul, M.A. and **Barras, B.F.** 1998: A geotechnical correction for post-depositional sediment compression: examples from the Forth valley, Scotland. *Journal of Quaternary Science* 13, 171–76.

Pejrup, M.C. 1988: The triangular diagram used for classification of estuarine sediments: a new approach. In de Boer, P.L., van Gelder, A. and Nio, S.D., editors, *Tide-influenced sedimentary environments and facies*, Dordrecht: D. Reidel, 289–300.

Queiroz, P. and **Mateus, J.** 1994: Preliminary palynological investigation on the Holocene deposits of Lagoa de Albufeira and Lagoa de Melides, Alentejo (Portugal). *Revista de Biologia* 15, 15–27.

Revel, M., Sinko, J.A. and **Grousset, F.E.** 1996: Sr and Nd isotopes as tracers of North Atlantic lithic particles: paleoclimatic implications. *Paleoceanography* 11, 95–113.

Rocha, F. 1993: Argilas aplicadas a estudos litoestratigráficos e paleoambientais na Bacia Sedimentar de Aveiro. Unpublished PhD Dissertation, University of Aveiro, 399 pp (available from author).

Schultz, L.G. 1964: Quantitative interpretation of mineralogical composition from X-ray and chemical data for the Pierre Shale. *US Geological Survey Professional Papers* 391–C, 1–31.

Silva, A. 1869: *Annaes do Municipio de Sant'iago do Cacem*. Lisboa: Imprensa Nacional, 280 pp.

Silvester, R. 1974: *Coastal engineering*, volume 2. Oxford: Elsevier, 338 pp.

Stuiver, M., Long, A., Kra, R.S. and **Devine, J.M.** 1993: Calibration – 1993. *Radiocarbon* 35.

Talma, A.S. and **Vogel, J.C.** 1993: A simplified approach to calibrating C14 dates. *Radiocarbon* 35, 317–22.

Thorez, J. 1976: *Practical identification of clay minerals*. Bruxelles: G. Lelotte, 99 pp.

Vogel, J.C., Fuls, A., Visser, E. and **Becker, B.** 1993: Pretoria calibration curve for short lived samples. *Radiocarbon* 35, 73–86.